Inorganic Chemistry Communications 155 (2023) 111122

Contents lists available at ScienceDirect

Inorganic Chemistry Communications

journal homepage: www.elsevier.com/locate/inoche

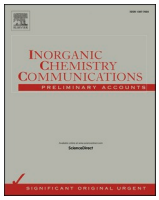

A new 1-D polymeric chains of $(C_5H_6ClN_2)[CdCl_3H_2O]\cdot H_2O$ perovskite: Synthesis, Structure, Physico-Chemical Characteristics, theoretical calculations, and biological effects

Sabrine Hermi [a], Mohamed Habib Mrad [b,*], Abdullah A. Alotaibi [b], Burak Tüzün [c], Uwe Böhme [d], Khalid M. Alotaibi [e], Abdelhak Othmani [f], Hamdy A. Hassan [g,h], Cherif Ben Nasr [a]

[a] Laboratoire de Chimie des Matériaux, Université de Carthage, Faculté des Sciences de Bizerte, 7021, Zarzouna, Tunisia
[b] Department of Chemistry, College of Sciences and Humanities, Shaqra University, 11911, Ad-Dawadmi, Saudi Arabia
[c] Plant and Animal Production Department, Technical Sciences Vocational School of Sivas, Sivas Cumhuriyet University, Sivas, Turkey
[d] Institut für Anorganische Chemie, TU Bergakademie Freiberg, Leipziger Str. 29, 09599 Freiberg, Germany
[e] Department of Chemistry, College of Science, King Saud University, Riyadh 11451, Saudi Arabia
[f] Laboratory of Material Physics: Structures and Properties, LR01 ES15, Faculty of Sciences, University of Carthage, Zarzouna, Bizerte 7021, Tunisia
[g] Department of Biological Science, Faculty of Science and Humanity Studies, Shaqra University, Al-Quwayiyah 11971, Saudi Arabia
[h] Department of Environmental Biotechnology, Genetic Engineering and Biotechnology Research Institute, University of Sadat City, Sadat City 32958, Egypt

ARTICLE INFO

Keywords:
1-D polymeric chains
Gap energy
DFT
Molecular docking
Swiss-ADME
Complex impedance spectroscopy
Antibacterial effect

ABSTRACT

A novel 1D polymeric chains material $(C_5H_6ClN_2)[CdCl_3H_2O]\cdot H_2O$ perovskite was successfully synthesized with the use slow evaporation process. According to the single-crystal X-ray diffraction, the structure was deduced to crystallize in the monoclinic system (space group $P2_1/n$, no 14), with the cell parameters a = 17.8596 (9) Å, b = 7.5766 (2) Å, c = 18.2245 (9) Å, and β = 95.068 (4)°. The crystal packing is composed of infinite polymeric chains of $[CdCl_3H_2O]^{n-}_n$, that form with the organic cations layers parallel to the (10–1) plane and are held together by multiple H-bonds and Van der Waals interactions. The supramolecular assembly was also explored by the Hirshfeld surface study. The IR spectroscopic investigations were described to confirm the organic group's existence and define the corresponding vibration modes. The optical study was also used to show the semiconducting behaviour of this compound, which showed relatively low gap energy 2.8 eV, promising for diverse applications especially in tandem solar cells. The Arrhenius relation may be used to explain the conductivity of the material. In addition, the graphs of Z' and Z'' versus frequency were a perfect match to an equivalent circuit model, which was represented as a resistance linked in series with two parallel circuits (R//CPE). The chemical properties of the studied metal complex were investigated, and the properties of nonlinear optical effects (NLO) were also calculated. The molecular docking approach was utilized to determine the studied compound's interactions with breast, lung, liver, and colon cancer proteins, which were then examined in detail with PLIP analysis. In contrast, the Swiss-ADME analysis was performed to examine its pharmacological properties. Pathogenic microorganisms like *Klebsiella pneumoniae* and *Staphylococcus aureus* were also used to test how well the cadmium complex and antibiotics work together.

1. Introduction

In recent years, the development of hybrid materials combining metal halides and organic molecules has attracted significant attention in the field of chemical research and material science [1]. Particularly, there has been a growing interest in hybrid compounds based on 2-aminopyridinium. These materials exhibit unique features and properties that make them highly promising for various applications in fields such as pharmaceuticals, photochemistry, electrochemistry, and catalysis [2–4]. One of the reasons for the selection of these hybrid compounds is the 2-aminopyridinium's ability to act as a hydrogen bond donor, while metal halides are renowned for their strong hydrogen bond

* Corresponding author.
E-mail address: m.mrad@su.edu.sa (M. Habib Mrad).

https://doi.org/10.1016/j.inoche.2023.111122
Received 4 February 2023; Received in revised form 6 July 2023; Accepted 21 July 2023
Available online 24 July 2023

accepting capabilities. When these components come together, they form solid-state assemblies that create molecular networks in one, two, or three dimensions through non-covalent interactions. These interactions include hydrogen bonding, π–π stacking, C–H…π interactions, as well as Van der Waals forces [5–8].

The choice of cadmium in the context of this study is based on its specific coordination numbers and geometries. Cadmium, in its Cd(II) state, possesses a d10 electronic configuration, which often results in complex geometries such as deformed tetrahedral, trigonal bipyramidal, and octahedral arrangements [9,10]. This vast diversity of geometries, coupled with the ability to form complexes with various types of ligands, makes cadmium complexes highly useful in the field of antimicrobials [11–13]. By complexing cadmium with antibiotics, the metal can effectively enter bacterial cells and exert its antibacterial activity [14]. In contrast to traditional organic antibiotics, mineral-based antibiotics offer a different range of modes of action. The novel mechanisms of action associated with mineral-based compounds, whether used alone or in combination with antibiotics, hold promise as effective treatments against bacterial infections that have developed resistance to conventional antibiotics. Consequently, utilizing mineral-based compounds alone or in combination with antibiotics provides additional modes of action that can enhance the effectiveness of treatment against resistant bacterial infections [15].

The main objective of this study was to synthesize and analyze a new cadmium-based hybrid compound (Cadmium Supramolecular Assembly (CSA)). The study encompassed various aspects, including the synthesis technique, atomic arrangement, and the investigation of vibrational, optical, and dielectric properties of CSA. Additionally, the study explored the antimicrobial screening synergy of antibiotics in combination with the cadmium compound. To understand the intermolecular interactions within the crystal packing of CSA, the researchers utilized Hirshfeld surface analysis, using the crystal information file (*.CIF). Furthermore, the chemical characteristics of CSA were examined through calculations at different levels: B3LYP, HF, and M062X, with the 3-21G, Lanl2DZ, and STO-3G basis sets [16–19]. The study also focused on the calculation of properties related to nonlinear optical effects (NLO) in metal complexes. For this purpose, the researchers employed the local hard-soft acid-base (HSAB) hypothesis, a prominent theory for explaining chemical reactivity and selectivity in compounds [20,21]. According to the computations, soft–soft interactions are preferred in the maximum Fukui function zone, whereas hard-hard interactions are preferred in the minimum Fukui function region [22,23]. Another significant aspect of the research was exploring the activity of the newly developed metal complex on cancer proteins, specifically breast (PDB ID: 1JNX), lung (PDB ID: 2H80), liver (PDB ID: 3WZE), and colon (PDB ID: 4UYA) cancer proteins [24–27]. Docking calculations were conducted to study the interactions occurring between the metal complex and these cancer proteins, and further analysis was performed using PLIP analysis. Lastly, the pharmacological characteristics of the synthesized compound were investigated through Swiss-ADME analysis to gain insights into its potential pharmaceutical applications.

2. Experimental

2.1. Method and synthesis

An aqueous solution of $CdCl_2$ (0.183 mg) was mixed with a solution of 3-amino-2-chloro-pyridine (0.064 mg) in water and a few drops of concentrated hydrochloric acid. After 7 h of constant stirring, the solution evaporated at ambient temperature. It took a week to isolate the stable crystals under normal temperature and humidity conditions.

The elemental analysis method was employed to ascertain the proposed formula of the obtained crystals (calc/found): C: (15.62%/15.73%), N: (7.29%/7.34%), H: (2.62%/2.70%).

2.2. Characterizations techniques

2.2.1. X-ray diffraction studies of $(C_5H_6ClN_2)[CdCl_3H_2O].H_2O$

The $(C_5H_6ClN_2)[CdCl_3H_2O]\cdot H_2O$ compound's single crystal X-ray diffraction data were taken using ω and φ scans on an STOE IPDS-2 T image plate diffractometer at room temperature with Mo-Kα radiation. X-AREA was used for data collection and cell refinement, and X-RED for data reduction [28]. **Table S1** summarizes crystal data and structural refinement information. The direct method was used to generate preliminary structure models, and SHELXL was used to refine the structure based on F^2 for all reflections [30]. The H atoms bound to oxygen atoms O1A, O2A, O1B, and O2B (water molecules) were located and refined using residual electron density maps. All remaining hydrogen atoms at calculated sites were included in the structural model and revised as they were constrained to the bound atoms.

2.2.2. Computational details

The results of theoretical simulations may provide very useful information on molecules' chemical and biological properties [31]. Theoretical simulations provide several quantum chemical parameters. The estimated parameters are used to describe the molecules' chemical activity. The Gaussian09 RevD.01 [32] and GaussView 6.0 [33] programs were used to do computations in the B3LYP, HF, and M06-2x approaches with the 3-21G, Lanl2DZ, and STO-3G basis sets [34–36]. As a direct result of these investigations, much information about quantum chemical parameters has been found. Each parameter describes a particular molecule's chemical property; the calculated parameters are calculated as follows [37]:

$$\chi = -\left(\frac{\partial \mathrm{E}}{\partial \mathrm{N}}\right)_{\upsilon(r)} = \frac{1}{2}(I+A) \cong -\frac{1}{2}(E_{HOMO}+E_{LUMO})$$

$$\eta = -\left(\frac{\partial^2 \mathrm{E}}{\partial \mathrm{N}^2}\right)_{\upsilon(r)} = \frac{1}{2}(I-A) \cong -\frac{1}{2}(E_{HOMO}-E_{LUMO})$$

$$\sigma = 1/\eta\omega = \chi^2/2\eta\varepsilon = 1/\omega$$

A technique exists for contrasting the biological actions of the metal complexes with those of proteins. Molecular docking is the most typical of them. Metal complexes can be compared using a few of these molecular docking techniques. The HEX 8.0.0 software is employed in this investigation. These enzyme proteins interact with the ligand and its metal complexes to boost their biological activity [38]. Molecules' biological activities were compared to those of enzymes using molecular docking calculations. At HEX 8.0.0, the enzyme and molecule files were examined [39].

For docking, the following variables are used: correlation type shape only, 3D FFT mode, 0.6-dimensional grid, 180-degree receptor and ligand ranges, 360-degree twist range, and 40-degree distance range. The interaction between the chemicals and the proteins was also thoroughly examined using the Protein-Ligand Interaction Profiler (PLIP) service [38]. It was also used to examine how the chemicals and proteins worked together.

This silico approach was used to do a virtual evaluation of the pharmacokinetics and drug-likeness of the cadmium metal complex, the only metal complex tested using this method. Additionally, the Swiss-ADME research attempts to make predictions about ADME characteristics such as molecular structure, as well as absorption, distribution, metabolism, and excretion [39,40]. Lipophilicity, topological polar surface area (TPSA), solubility (log S), a fraction of sp3 hybridization carbon, and rotatable bonds were considered in developing the radar of durability, which was used to evaluate the drug-like potential of the compound. Numerous additional factors were computed and investigated, including physicochemical and pharmacokinetic ones that safeguard organisms and tissues.

2.2.3. FT-IR, UV–vis measurements

The FT-IR spectra of the compound; $(C_5H_6ClN_2)[CdCl_3H_2O]\cdot H_2O$ were collected using a KBr pellet and a Perkin Elmer L120-00 spectrometer in the wavenumber range of 4000–400 cm^{-1} (with a resolution of 2 cm^{-1}). On the other hand, the optical characteristics were measured at room temperature using a Perkin-Elmer-Lambda 11UV/Vis spectrophotometer. The measurements were taken between the wavelengths of 500 and 150 nm.

2.2.4. Dielectric properties

Electrical measurements of the real and imaginary components of the impedance characteristics (Z' and Z") were done on pellet disks with a diameter of approximately 8 mm and a thickness of 1.3 mm using a Hewlett-Packard HP 4192 A analyzer.

2.2.5. Bactericidal activity

This compound's antibacterial activity was evaluated. The cadmium complex was tested for synergistic activity against pathogenic bacteria *Klebsiella pneumoniae* and *Staphylococcus aureus* with antibiotics (Norfloxacin (NOR-10), Novobiocin (NV-5), Erythromycin (E-15), and Nalidixic acid (NA30). 20 μL of each bacterial strain inoculum suspension was swabbed on Mueller–Hinton agar. Discs with a 4-mm diameter were immersed in the metal complex using four dilutions of 12.5 $\mu g.mL^{-1}$ and doubled to 100 $\mu g.mL^{-1}$ four immersed discs in the four dilutions were tested for their antibacterial activity for the two strains in this study, *K. pneumonia* and *S. aureus*. Plates were incubated for 20 min at room temperature, followed by 24 h at 30 °C. The synergistic effect of 100μgmL^{-1} solution metal complex, and the antibiotic discs from NV-5, E-15, NOR-10, and NA30, was tested. The inhibition zone diameters for the metal complex either alone or with the antibiotic discs, where the antibiotic discs from NV-5, E-15, NOR-10, and NA30 were used as positive control.

3. Results and discussion

3.1. Crystal structure description of $(C_5H_6ClN_2)[CdCl_3H_2O].H_2O$

The ORTEP representation of the $(C_5H_6ClN_2)[CdCl_3H_2O].H_2O$ is shown in Fig. 1. It consists of two $C_5H_6N_2Cl^+$ cations (A and B), two crystallization water molecules, and two cadmium atoms, Cd1A and Cd1B, each surrounded by three chlorine atoms and coordinated water.

The $(C_5H_6ClN_2)[CdCl_3H_2O].H_2O$ compound is made by applying the glide plane ***n***, the two-fold screw axis, and inversion center operation to the unit regularly. In fact, the $[CdCl_3H_2O]_n^{n-}$ anions form a three-dimensional porous anionic network with 1D channels by self-assembling with the nearest water molecules O2A and O2B. Consequently, the resulting porous structure has voids; when combined with inorganic molecules, the organic molecules act as bridges and neutralizers. It is noted that the 3-amino-2-chloropyridinium cations are held to the polymeric chains via N—H…O, N—H…Cl, and C—H…Cl H-bonds to form the tridimensional network (**Figure S1**).

Cadmium atoms Cd(1A) and Cd(1B) occupy a special position on the two-fold screw axis of the $P2_1/n$ space group, generating endless chains of $[CdCl_3H_2O]_n^{n-}$ parallel to the $\vec{b}$ direction. In fact, each cadmium Cd (II) atom is surrounded by five chlorine atoms and a water molecule giving rise to two octahedra, each one containing two bridging chlorine atoms, Cl (3A) and C1 (4A) of $[Cd(1A)Cl_3H_2O]_n^{n-}$ and Cl (3B) and Cl (4B) of $[Cd(1B)Cl_3H_2O]_n^{n-}$. Figure S2 of the supplementary information displays the polymeric chains $[Cd(1A)Cl_3H_2O]_n^{n-}$ and $[Cd(1B)Cl_3H_2O]_n^{n-}$. The distance between successive metal atoms in the $[Cd(1A)Cl_3H_2O]_n^{n-}$ chain is 3.814 Å, and the angle Cd–Cd–Cd is 166.73°. On the other hand, the Cd–Cd distance in the $[Cd(1B)Cl_3H_2O]_n^{n-}$ chain is 3.795 Å, and the angle of Cd–Cd–Cd is 173.11°, suggesting that the polymer chains are almost linear. The interatomic distances and bond angles of the inorganic part of $(C_5H_6ClN_2)[CdCl_3H_2O]\cdot H_2O$ are shown in Tables S2 and S3. These values are equivalent to those obtained for other halocadmate systems found in the literature [41–43]. The average distortion parameters were computed using (1) and (2) [44]:

$$\mathbf{ID(Cd-Cl)} = \sum_{i=1}^{n1} \frac{|\mathbf{di-dm}|}{\mathbf{n1dm}} \quad (1)$$

$$\mathbf{ID(Cl-Cd-Cl)} = \sum_{i=1}^{n2} \frac{|\mathbf{ai-am}|}{\mathbf{n2am}} \quad (2)$$

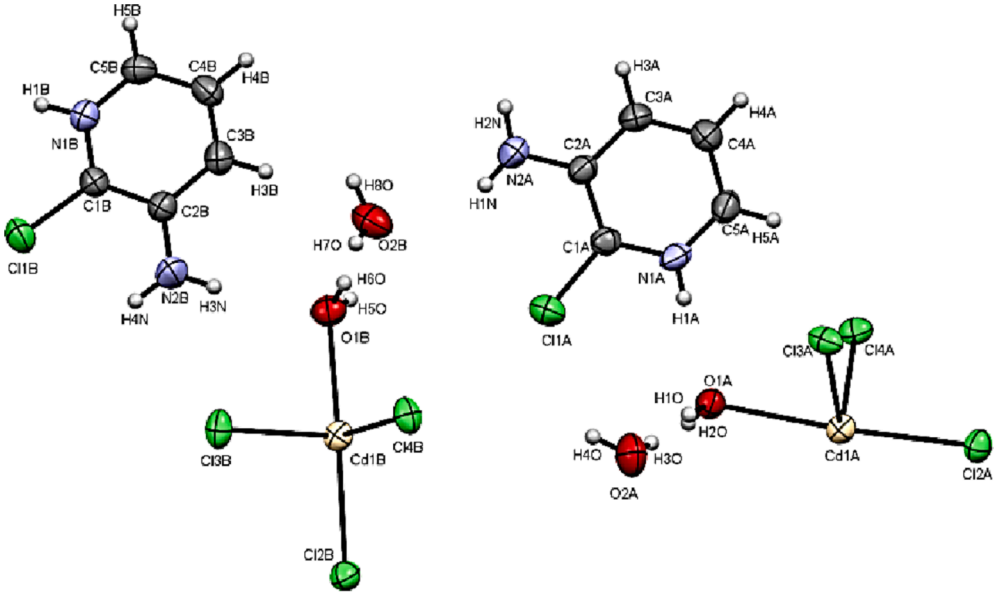

Fig. 1. The ORTEP presentation of the geometric configuration of $(C_5H_6ClN_2)[CdCl_3H_2O]\cdot H_2O$.

The value of the distortion indices were ID(Cd-Cl) = 0.044 and ID(Cl-Cd-Cl) = 0.0026 for $[Cd(1A)Cl_3(H_2O)]^-$ and ID(Cd-Cl) = 0.063 and ID (Cl-Cd-Cl) = 0.0026 for $[Cd(1B)Cl_3(H_2O)]^-$. The interaction of the organic groups and the water molecules with the chloride pairs and the coordinated water molecules probably caused these values.

As seen in Fig. 2**. a** and **2. b**, the organic cations seem to be positioned on both sides of the polymeric chains, forming layers parallel to the (−1 0 1) planes. The crystal packing is more stable owing to the H-bonds (**Table S4**) and the intermolecular π… π stacking between adjacent antiparallel aromatic rings and the π…Cl interactions (Fig. 3**).**

The geometric properties of $(C_5H_6N_2Cl)^+$ indicate no significant variations from those found in other materials containing the same organic groups (**Table S3**) [2,3,45]. Indeed, the organic geometrical properties demonstrate that they have many similarities, including a nearly planar pyridyl ring that creates an inclined dihedral angle with the amino group (4.550° and 1.169°, respectively, for cations A and B) (**Figure S3**). The amino groups in the two cations are planar, and the lengths of the C-N bonds (1.346 (1) Å for A and 1.333 (1) Å for B) are shorter than in pyridine (1.367 (2) Å). Moreover, the C1A–N1A–C5A (123.18°) and C1B–N1B–C5B (123.43°) bond angles are wider than that in pyridine (116.94°), which indicates the protonation of the pyridine ring's N atom. These findings also suggest that the amino group and the pyridine ring have a strong conjugation [46].

The crystal structure of $(C_5H_6ClN_2)[CdCl_3H_2O].H_2O$ ate deviates from the traditional ABX3 perovskite composition but displays structural motifs reminiscent of perovskite-like frameworks. It features a three-dimensional porous anionic network formed by $[CdCl_3H_2O]^{n-}_n$ anions, which create one-dimensional channels throughout the crystal lattice. The $(C_5H_6N_2Cl)^+$ cations act as bridges within the porous structure, forming a tridimensional network through hydrogen bonding interactions. The cadmium atoms Cd(1A) and Cd(1B) form endless chains of $[CdCl_3H_2O]^{n-}_n$ running parallel to the *b*-axis, with distorted octahedral coordination geometries. The crystal structure also exhibits stacking of perovskite-like layers and intermolecular interactions such as hydrogen bonding and π…π stacking. Overall, although it deviates from the conventional ABX3 perovskite composition, the crystal structure demonstrates intriguing perovskite-like characteristics.

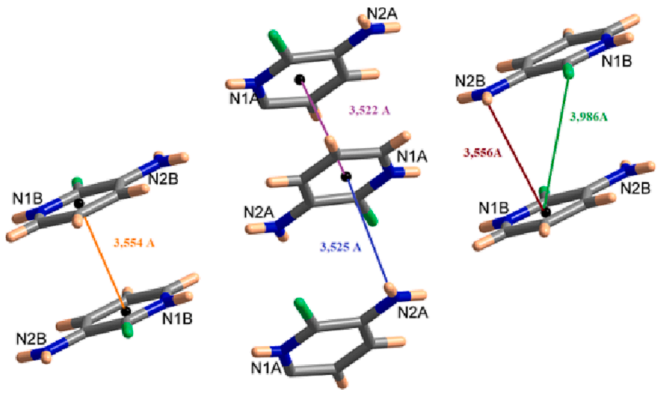

Fig. 3. Representation of the different intermolecular contacts between aromatic rings.

3.2. Hirshfeld surface study

For crystallographers, the Hirshfeld surface analysis is fundamental because it offers vital details regarding various non-covalent interactions that influence molecular packing in crystals [47]. The molecular environment around the d_{norm} representation of $(C_5H_6ClN_2)[CdCl_3H_2O]\cdot H_2O$ molecules is shown in Fig. 4**.a**. The surface's transparency enhances the visibility of the molecular components. The defined pattern of neighboring blue and red triangles on the shape index surfaces (Fig. 4**.b**) and a wide and flat green area on the same side of the related curved surfaces (Fig. 4**.c**) evidence stacking interactions exist.

The 2D fingerprint plots illustrated the interactions' contributions to the crystal structure. The H…Cl/Cl…H contacts, which are related to hydrogen bonds (**Table S4**) in the structure, are responsible for the most important contribution, as shown by the two peaks indicating strong H-bonding interactions in the 2D plot (**Figure S4.a**) owing to the significant amount of hydrogen and chlorine on the surface (% S_H = 52.75% and % S_{Cl} = 38.05%). According to Table 1, this type of interaction has an E_{HCl} greater than unity (E_{HCl} = 1.48). Moreover, the H…H interactions are the second most prevalent kind of interaction, where they occupy the central area of the 2D map and represent 17.7% of the entire Hirshfeld surface (**Figure S4.b**). The involvement of hydrogen atoms in hydrogen bonds between cationic and anionic moieties, with these contacts, are slightly underrepresented, causing an enrichment rate of

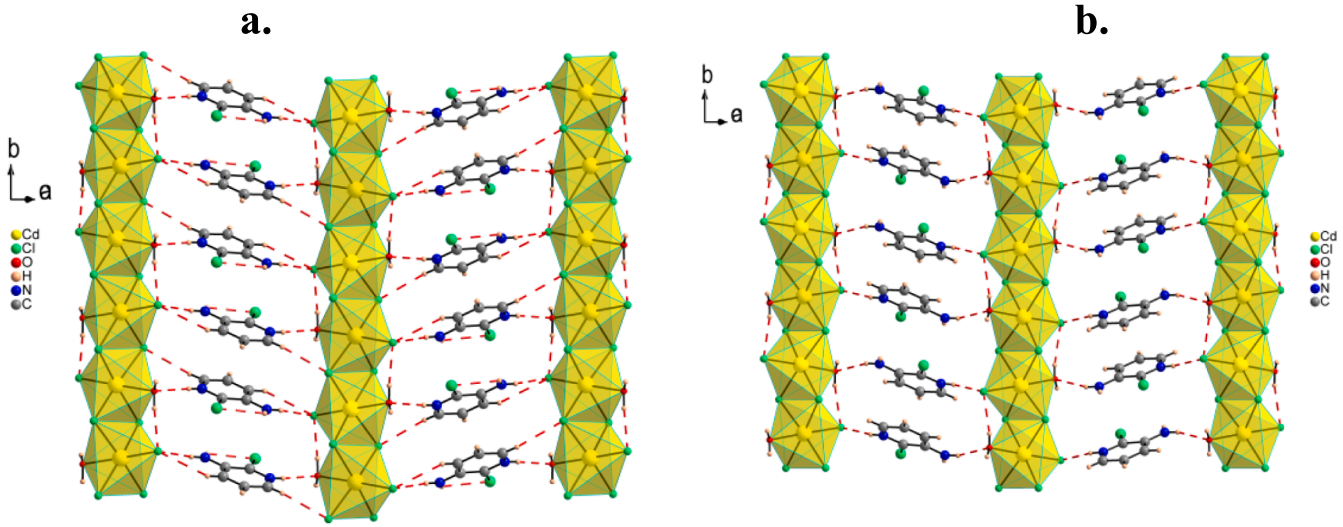

Fig. 2. Projection of the layer formed by the polymeric chains $[Cd(1A)Cl_3H_2O]^{n-}_n$ and the cations A (a). Projection of the layer formed by the polymeric chains $[[Cd(1B)Cl_3H_2O]^{n-}_n$ and the cations B.

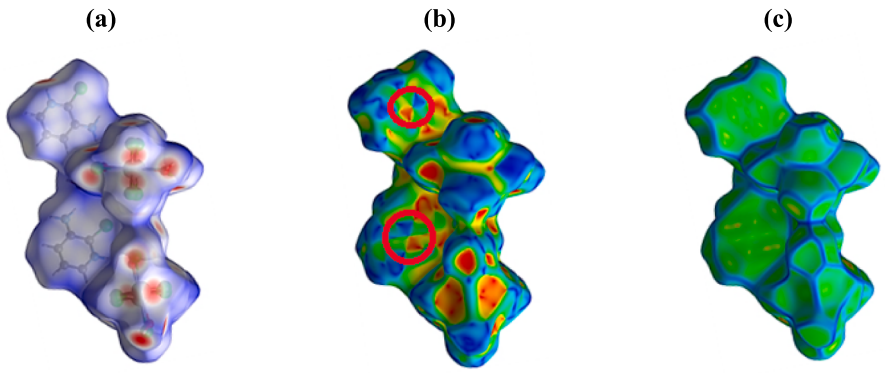

Fig. 4. Representation of the 3D Hirshfeld surface plotted over the d_{norm} (a), Shape index (b), and Curvedness (c).

Table 1
The $(C_5H_6ClN_2)[CdCl_3H_2O]\cdot H_2O$ compound's enrichment ratios and chemical proportions on the Hirshfeld surface.

Atoms	H	Cl	C	O	Cd	N
%Surface	**52.75**	**38.05**	**2.7**	**4.7**	**1.35**	**0.4**
H	0.63	1.48	0.42	1.69	0.14	/
Cl	–	0.44	0.34	0.11	2.43	0.32
C	–	–	/	1.18	0	/
O	–	–	–	0	0	0
Cd	–	–	–	–	0	0
N	–	–	–	–	–	0

/ : Enrichment ratios for random contacts lower than 0.9% are not shown because they are not meaningful.

0.63. The H…O/O…H interactions are the third most significant contacts, accounting for about 8.4% (**Figure S4.c**) and having an enrichment ratio greater than unity (E_{HO} = 1.69; Table 1). In the two-dimensional fingerprint plot, the Cl…Cl auto contact represents 6.4% of the total Hirshfeld surface (**Figure S4.d**) with an E_{ClCl} = 0.44. The percentage of Cd…Cl/Cl…Cd contacts 2.5%, shown as a single sharp wing, indicating strong interactions (**Figure S4.e**). This type of contact is considered the most favorable contact among all other contacts in the crystal package (E_{CdCl} = 2.43). It is worth mentioning the existence of weak interactions (less than 2 % contribution) such as C…H, C…C, Cl…C, C…N, N…H, Cl…O, Cl…N contributes less to the structure (**Figure S5**). In conclusion, this study, compatible with the X-ray diffraction investigation, provides a new visual explanation of intermolecular interactions.

3.3. Quantum descriptors

Theoretical calculations are important to quickly and easily compare molecules' activities. First, many quantum chemical parameters are calculated due to Gaussian calculations. Each of these calculated parameters explains many different properties of molecules and provides information about molecules with these properties in **Table S5**. Among these parameters, two important ones allow the activities of molecules to be compared: the HOMO and LUMO parameters. The HOMO value indicates a molecule's capacity to give electrons. The molecule that has the biggest positive numerical value for this attribute is the one that exhibits the highest level of activity [48]. The second parameter is the molecules' LUMO; this parameter's numerical value shows the molecules' electron-accepting ability, and the numerical value of the molecule with the most negative value has the highest activity [49]. Apart from these parameters, another calculated parameter is the ΔE parameter, which is known to have high activity if the numerical value is low [48]. The low value of this value facilitates electron transfer. The ability of each of the atoms that form a bond to attract bond electrons is called electronegativity, and this parameter's numerical value is known to have the greatest activity of any of the smallest molecules [49]. Many properties of molecules are examined with the calculations made. Another calculated parameter is chemical hardness and softness, which are important parameters that express the measure of reactivity and stability [21]. Softness, which is the opposite of chemical hardness (1/η), expresses the polarization property of molecules. Soft molecules are more reactive than hard molecules, and the reason for this is that soft molecules readily donate electrons to other molecules [48].

Few calculated parameters have visual representations, even though numerous parameters have been collected. The parameters obtained from the visualizations are given in Fig. 5. The first illustration, in this case, provides the molecules' optimal structures. The positions of the molecules' HOMO and LUMO orbitals are shown in the second and third illustrations, respectively, followed by a map of the molecule's molecular electrostatic potential. The red areas in this illustration are those with the greatest electron densities. The lowest electron density, however, is seen in the blue-colored zones [21].

Considering the thermodynamic values in the formation of the complex, it consists of the combination of three different molecules that form the complex molecule. The studied complex combines 2-chloropyridin-3-amine (A), water (B), cadmium chloride (C), and Complex (D). The energy (E), enthalpy (H), and Gibbs energy (G) values of each molecule were calculated. These values of the complex were calculated from these values, which were calculated afterward.

$$\Delta E = E_{complex} - ((E_{CdCl_2}*2) + (E_{water}*3) + (E_{ligand}*2))$$

$$\Delta H = H_{complex} - ((H_{CdCl_2}*2) + (H_{water}*3) + (H_{ligand}*2))$$

$$\Delta G = G_{complex} - ((G_{CdCl_2}*2) + (G_{water}*3) + (G_{ligand}*2))$$

The energy, the enthalpy, and the Gibbs free energy change values of molecules are calculated using the abovementioned formula (Table 2). The Gibbs free energy of the molecules allows us to determine whether or not this complex may form. If this Gibbs free energy value is less than zero, this complex will form spontaneously. If this value is equal to zero, the system is in equilibrium. If this value is greater than zero, the formation of this complex is in the direction of the reactants [49,50].

3.4. NLO properties

Investigating metal complexes' nonlinear optical effects (NLO) requires calculating many quantum chemical parameters. NLO is done to provide fundamental operations for emerging technologies in fields such as telecommunications, signal processing, and optical interconnects. These fundamental operations include optical modulation, frequency shifting, optical logic, optical switching, and optical memory [52]. Every determined metric provides crucial details about the molecules. These numerically measured characteristics, polarizability (α) and hyperpolarizability (β) are estimated to forecast the nonlinear optical

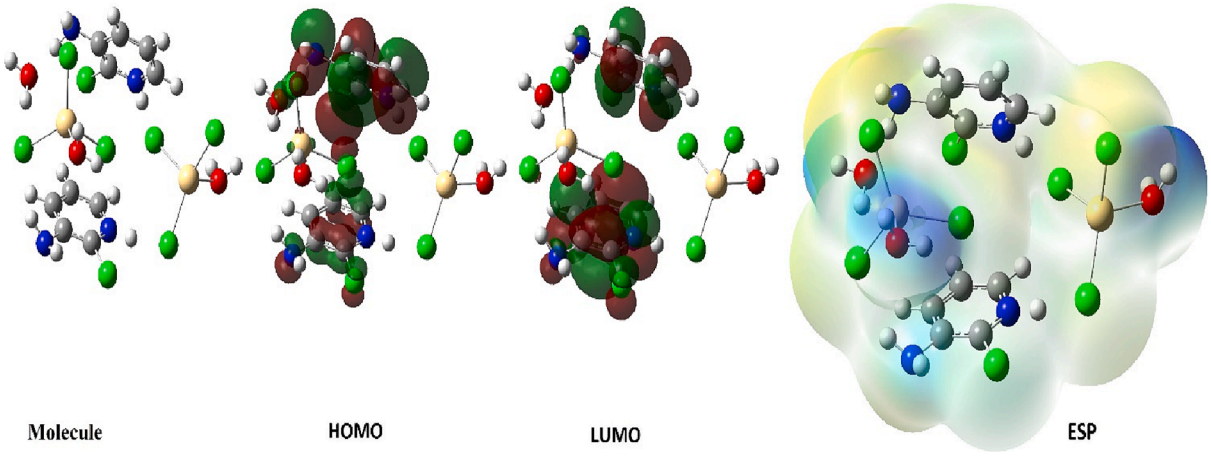

Fig. 5. Representations of optimizing the structure, HOMO, LUMO, and ESP of $(C_5H_6ClN_2)[CdCl_3H_2O]\cdot H_2O$.

Table 2
Thermodynamic values of $(C_5H_6ClN_2)[CdCl_3H_2O]\cdot H_2O$.

	E	H	G
2-chloropyridin-3-amine (A)	−8589.0123	−8588.9866	−8590.0272
Water (B)	−2067.6850	−2067.6593	−2068.2403
cadmium(III) chloride (C)	−2474.7772	−2474.7515	−2475.8287
Complex (D)	−28359.2034	−28359.1777	−28362.6792
Δ value	−28.5694	−28.7235	−26.2465

properties of materials. Polarizability and hyperpolarizability make up the two components of the dipole moment (μ) parameter for molecules. The parameters listed in the Table 3 below can be used to compute the NLO characteristics of molecules:

After calculating the polarizability (α_0) and hyperpolarizability (β_{tot}) values of the compounds, the atomic unit (a.u.) were multiplied by constant values in order to transform these estimated characteristics into electrostatic units ($\alpha : 1\,\text{a.u.} = 0.148\text{x}10^{-24}\text{esu}$ and $\beta : 1\,\text{a.u.} = 8.639\text{x}10^{-33}\text{esu}$). The features of NLOs change when the dipole moment, linear polarizability, polarizability anisotropy, and initial hyperpolarizability increase. These characteristics, listed in Table 3, were computed using the HF/Lanl2DZ basis set for the metal complex.

3.5. Molecular docking of $(C_5H_6ClN_2)[CdCl_3H_2O].H_2O$

In this research, molecular docking was used as a comparative approach for the activities of metal complexes. These activities analyze the interactions of various molecules with various proteins via calculations. An increase in these interactions is correlated with a rise in the activities of metal complexes. The total energy value, one of the calculated parameters of the metal complex studied as a result of the calculations, is an important parameter used to compare the activities of the molecules [53]. The highest molecular activity is known to be the one whose value for this parameter is the most negative. The total energy values of molecules calculated against various proteins are given in Table 4 and **Figures S6-S9**.

For this reason, PLIP analysis was used to investigate other interactions more deeply. The numerical values of the interactions between the metal complex and the proteins were obtained in **Tables S5-S8** and Fig. 6**.a, 6.b, 6.c, and 6.d**.

Table 3
NLO parameter values of $(C_5H_6ClN_2)[CdCl_3H_2O]\cdot H_2O$.

	a.u.	esu		a.u.	esu
α_{xx}	252.1308	3.731×10^{-23}	β_{xxx}	241.6595	$2.088\ \text{x}10^{-27}$
α_{xy}	0.6980	1.033×10^{-25}	β_{yyy}	−67.0853	$-5.797\ \text{x}10^{-27}$
α_{yy}	191.6689	$2.836\ \text{x}10^{-23}$	β_{zzz}	53.6949	$4.640\ \text{x}10^{-28}$
α_{xz}	−19.2838	$-2.854\ \text{x}10^{-24}$	β_{xyy}	−10.7966	$-9.329\ \text{x}10^{-29}$
α_{yz}	2.8128	$4.162\ \text{x}10^{-25}$	β_{xxy}	10.0063	$8.646\ \text{x}10^{-29}$
α_{zz}	225.4650	$3.336\ \text{x}10^{-23}$	β_{xxz}	−32.6333	$-2.820\ \text{x}10^{-28}$
Δ_{α}	252.1308	$3.731\ \text{x}10^{-23}$	β_{xzz}	30.1038	$2.601\ \text{x}10^{-28}$
μ_x	1.0009		β_{yzz}	100.7359	$8.705\ \text{x}10^{-28}$
μ_y	−0.3052		β_{yyz}	−162.8598	$-1.407\ \text{x}10^{-27}$
μ_z	0.4526		β_{total}	300.1936	$2.594\ \text{x}10^{-27}$
μ_g	1.1401				

3.6. Swiss-ADME analysis

Swiss-ADME analysis was used to study the ADME features of the studied metal complexes (**Table S9**). Many pharmacological and pharmacokinetic properties of metal complexes were investigated. Fig. 7 shows the six physicochemical indexes of the bioavailability radar, axis lipophilicity, size, polarity, solubility, flexibility, and saturation. All six physicochemical indexes of complex 1 appear to be better than complex 2. It is expressed as the value of the log P o/w of the molecules, a typical indicator of lipophilicity and the partition coefficient between octane and water solvents throughout the pharmacokinetic route. In addition to these factors, it is important to investigate how the researched metal complexes interact with certain pharmacokinetic proteins. Some examples of these proteins are P-glycoprotein (P-gp) and cytochrome P450 (CYP) [54]. It is well known that the primary function of P-gp is to protect the central nervous system from exposure to xenobiotics.

On the other hand, certain cancer cells release this protein, which is a contributing factor in the development of tumors that are resistant to treatment. From a pharmacological perspective, understanding how these drugs interact with cytochrome P450 (CYP) is of great value. It has been hypothesized that CYP and P-gp may collaborate to digest small molecules in a way that is synergistic to promote tissue and organism protection. This set of isoenzymes plays a crucial part in the metabolic process of drug clearance. In addition, the parameter also provides the skin permeability coefficient, denoted by the log Kp value. This value is determined by the size of the metal complexes in proportion to their lipophilicity [55].

The Boiled-Egg relationship between WLOGP and TPSA is used to

Table 4
E_{total} energy value of molecular docking parameter for the metal complex.

	Metal complex
Breast cancer protein	−257.80
Lung cancer protein	−303.92
Liver cancer protein	−294,73
Colon cancer protein	−297.65

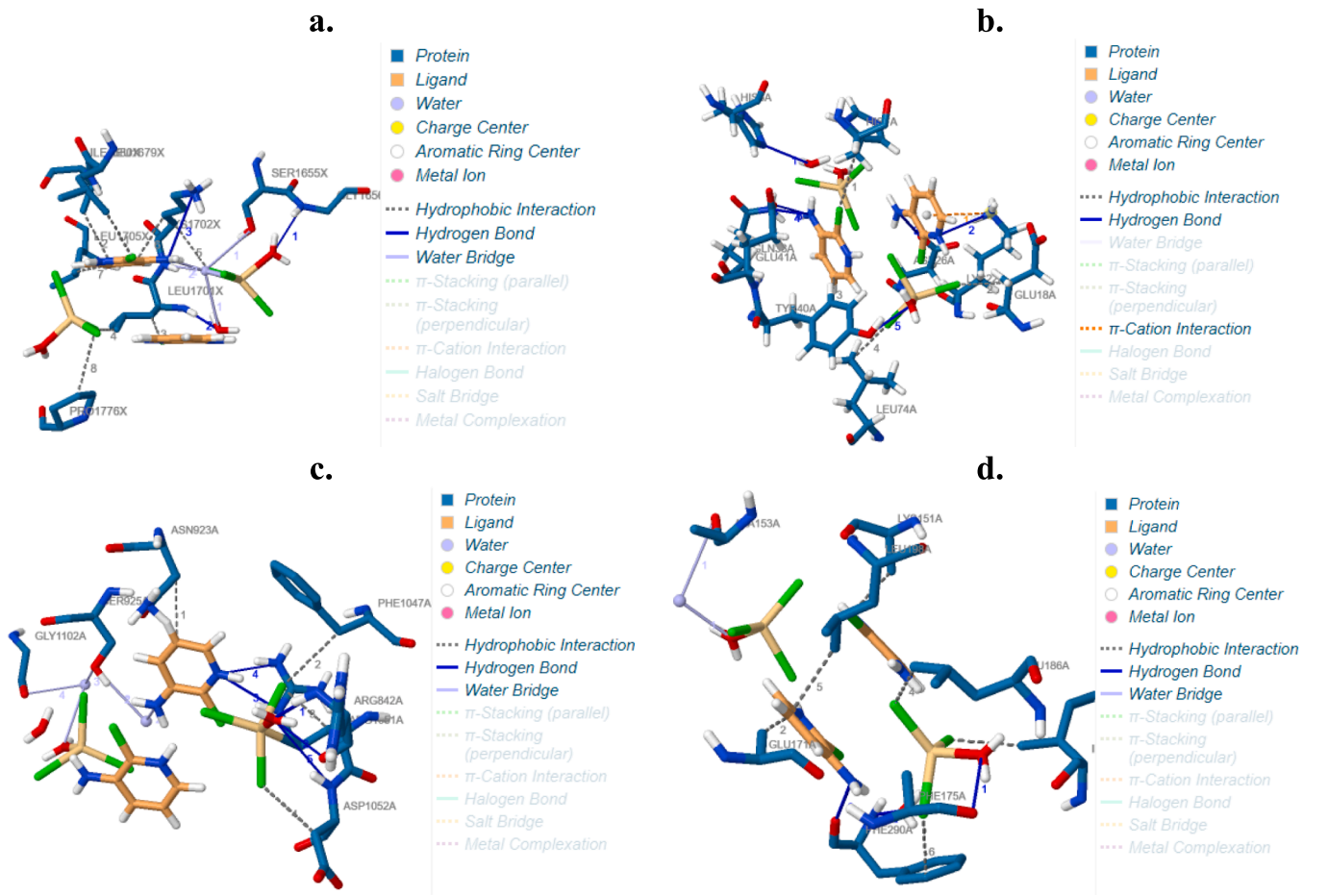

Fig. 6. Illustration of the metal complex's association with breast cancer (a), lung cancer (b), liver cancer (c), and colon cancer (d) proteins.

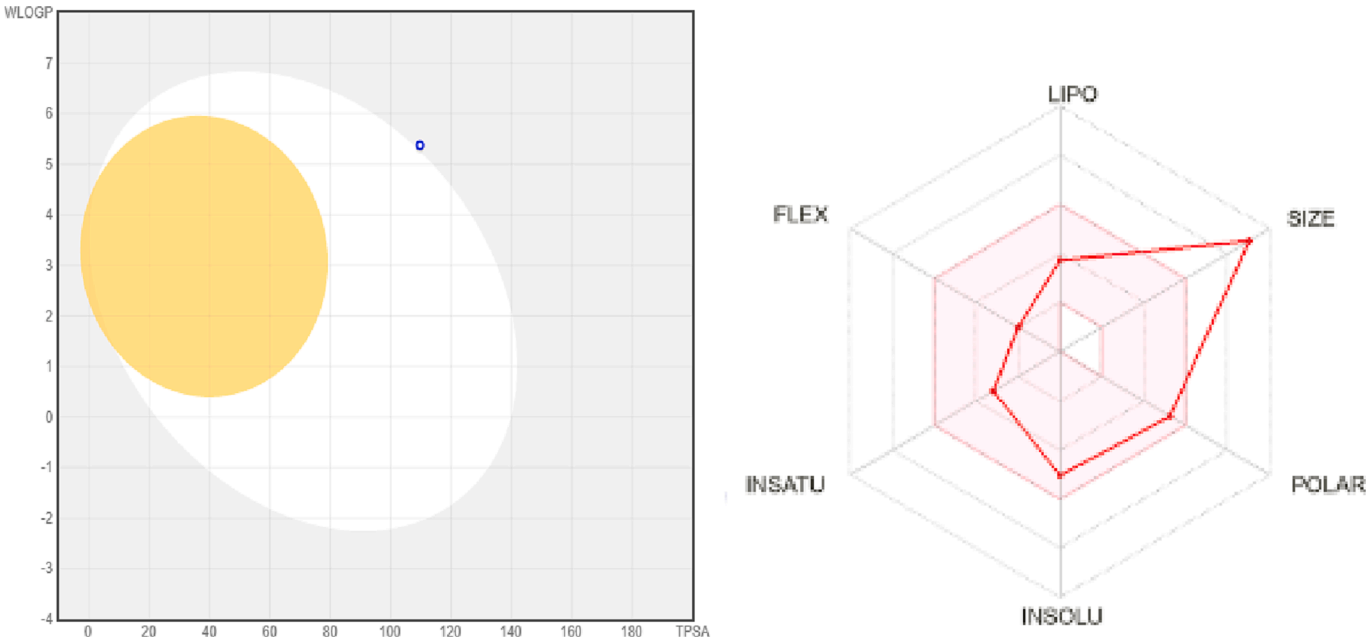

Fig. 7. Drug likeness parameters of the cadmium metal complex.

examine HIA (Human Intestinal Absorption) and BBB (Blood-Brain Barrier) as indications of passive gastrointestinal absorption and the blood–brain barrier, respectively. According to the Boiled Egg model calculations, the white region in Fig. 7 suggests a high possibility of passive absorption via the gastrointestinal system, whereas the yellow area (yolk) indicates a high probability of brain penetration.

3.7. Infrared spectroscopy

The functional groups in $(C_5H_6ClN_2)[CdCl_3H_2O]\cdot H_2O$ was confirmed using FTIR spectroscopy, and their solid-state vibrational behavior was compared to that of analogous compounds that contained the same organic cation (**Figure S10**) [2,3]. Broad bands in the range 3450–3100 cm^{-1} are derived from asymmetric and symmetric stretching vibrations of hydroxyl OH and NH_2 groups. The C–H stretching vibrations generally appear between 3000 and 3100 cm^{-1}. Similarly, the in-plane C–H bending vibrations appear within the range of 1376– 1134 $cm^{-1,}$ and the out-of-plane bending vibrations occur in the frequency range of 1051–800 cm^{-1}. The stretching vibration of C = N of the pyridine ring is presumably assigned at about 1589 cm^{-1} in the FTIR spectrum. The C–C stretching vibrations for rings are found between 1600 and 1400 cm^{-1}, in which the band located at 1638 cm^{-1} is ascribed to C = C stretching. The absorption peak situated at 694 cm^{-1} most probably corresponds to the deformation vibration of the pyridine ring. The stretching vibrations of C–Cl mode were allocated at 866 and 796 cm^{-1}. The wavenumbers between 925 and 600 cm-1 are attributed to (C–C–N) and (C–C–C) deformation. The C—N torsional modes are observed in 550–502 cm^{-1}.

3.8. UV spectroscopy

Figure S11 displays the UV-absorption spectrum in the solid state and at an ambient temperature of $(C_5H_6ClN_2)[CdCl_3H_2O]\cdot H_2O$ [56]. The organic part's π-π* transitions are responsible for the absorption bands at 228 nm. The bands in the compound's UV absorption spectrum, seen at 251 nm and 328 nm, are attributed to the conduction band's maximal energy level being absorbed, revealing the gap in the material. The band at 251 nm is primarily generated by the absorption between O (2 s or 2p) and Cd (5 s) (band to band) (5 s), while the absorption at 370 nm is attributable to the excitation of free electron-hole pairs as a result of the absorption between Cl (3p) and Cd (5 s).

The Tauc equation was used to compute the gap energy (Eg) of $(C_5H_6ClN_2)[CdCl_3H_2O]\cdot H_2O$, which was used to investigate the material's conduction type [57]. The linear interpolation on the x-axis of the graphical presentation $(\alpha h\nu)^2$ allows for determining the optical band gap energy, estimated to be 2.8 eV, as shown in **Figure S11**. These gap energy values in this material may be categorized as semiconductors and comparable to those of analogous compounds [58].

3.9. Complex impedance analysis

One of the crucial experimental techniques used to provide knowledge about the relaxation process is the investigation of the dynamics of ionic mobility in solids using complex impedance formalism. It also makes it possible to determine other properties like activation energy and the conductivity of materials [59,60]. The pattern of Z' vs. Z'' obtained throughout the frequency range of 5——13 MHz at various temperatures (290 K to 408 K) is shown in Fig. 8. **a**. The experimental data were fitted and adjusted by the EC-Lab fitting software. Fig. 8. **b** displays the Nyquist plot of $(C_5H_6ClN_2)[CdCl_3H_2O]\cdot H_2O$ achieved at 368 K and the corresponding fitted data. A resistance coupled in series with two parallel (R/CPE) circuits accurately describes the compound's equivalent circuit. Low-frequency semicircles represent the grain boundary effect, whereas high-frequency semicircles represent the bulk (grain) of the material. The intercepts of the semicircles on the real axis are the grain resistance (Rg) and grain boundary resistance (Rgb) related to the experimental temperature. It is important to notice that when temperatures increase, Rg and Rgb increase [61–64].

Investigation of Fig. 9 reveals the impedance increases instead of decreasing between temperatures of 323 K and 363 K. Consequently; the measurements were carried out again, focusing on those at 323 K. The sample was maintained at 324 K for 24 h, and the impedance was measured at different times. Fig. 9 shows the complex impedance spectra measured when the oven temperature reached 323 K after 10

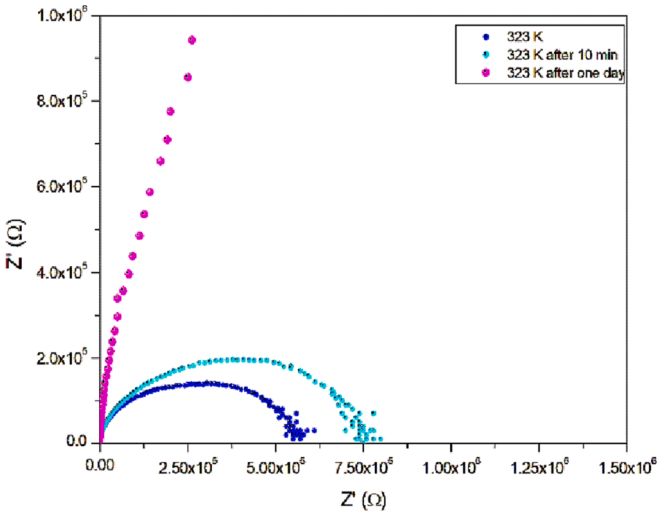

Fig. 9. Time dependence of complex impedance spectra at 323 K.

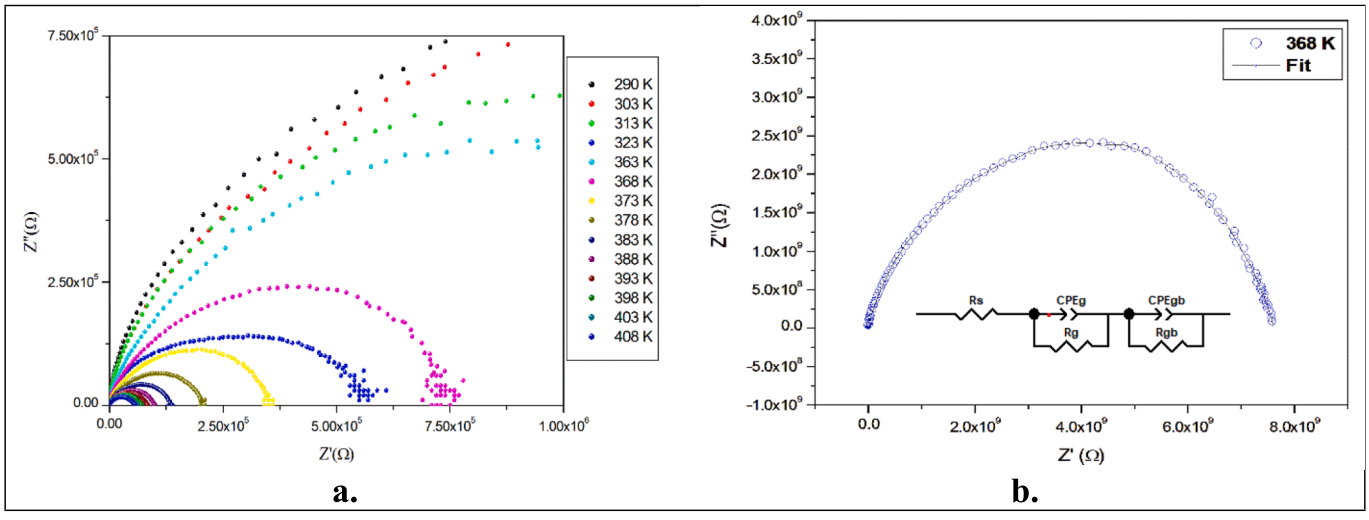

Fig. 8. Impedance spectra, complicated at various temperatures (a), Nyquist diagrams at 368 K, and the equivalent circuit model of $(C_5H_6ClN_2)[CdCl_3H_2O]\cdot H_2O$.

min. and 24 h later. It is observed that the impedance significantly increases, indicating that the mechanism of conduction changes over time. Our material contains hydrogen bounded water molecules, which can evaporate at 323 K [65]. Consequently, We believe that the evaporation of hydrogen bouded water molecules causes the change of the conduction mechanism between 323 and 368 K.

Figure S12 show the frequency-dependent fluctuation of the real (Z') and imaginary (Z") impedance components of $(C_5H_6ClN_2)[CdCl_3H_2O]\cdot H_2O$ at various temperatures. In fact, when the temperature rises, the amplitude of Z" drops and the peak frequency moves to higher values, causing the relaxation times to become thermally active. The broadness of the peaks suggests that the system has undergone several periods of relaxation. The relaxing process may be triggered by the presence of immobile species at low temperatures and defects at high temperatures [63,64].

We use the Arrhenius modeling equation to comprehend the conduction phenomena in $(C_5H_6ClN_2)[CdCl_3H_2O]\cdot H_2O$ [66]:

$$\sigma T = A\, e^{E_a/k_bT}$$

where: E_a is the activation energy, kb is the Boltzmann constant, σ represents the conductivity, and A is the preexponential factor. Fig. 10 depicts the temperature development of the compound's specific conductivity σT vs. 1000/T, which indicates an Arrhenius-type behavior. A discontinuity in the linear curve's slope is seen between 323 K and 363 K, and around 380 K, a shift in slope was noticed. Subsequently, there are three distinct zones of conductivity, labeled (I), (II), and (III), with the activation energies in areas Ea (I) = 0.53 eV, Ea (II) = 3.13 eV, and Ea (III) = 3.13 eV. The thermally activated mechanism explains the conduction in this manner [63].

The investigation of electrical characteristics has utilized the complex modulus formalism since it captures the primary responsibility of the polycrystalline bulk. In addition, it is ideal for extracting information such as electrode polarization and conductivity relaxation durations [67,68]. When analyzing the data in modulus format, M' tends to be extremely small at lower frequencies, demonstrating that the electrode effects have little impact and may thus be disregarded. Additionally, it exhibits an extremely low value of M' (0) in the low-frequency domain. For all temperatures, a continuous dispersion with frequency increase tends to saturate at a maximum asymptotic value denoted by M in the high-frequency zone, showing a relaxation process covering a variety of frequencies. The polycrystalline's best fits for M" at various temperatures are shown in **Figure S13**. Due to the distributed nature of the frequencies involved in the relaxing processes, M" approaches a constant value at high frequencies for all temperatures [59]. This graph shows three main areas near one another, demonstrating three conduction zones.

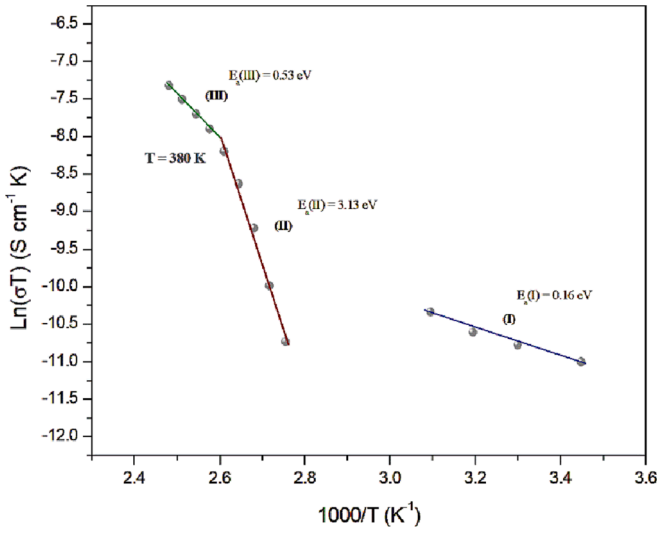

Fig. 10. Dependence of Ln(T) on the temperature in comparison to the reciprocal temperature of $(C_5H_6N_2Cl)[CdCl_3(H_2O)]\cdot H_2O$.

The activation energy value obtained for our compound suggests similarity to translocative proton conductors, indicating proton transfer through propagation along H-bonding chains rather than pure ionic diffusion. Moreover, the crystallographic study revealed a three-dimensional H-bonding network, resulting in higher conductivity compared to lamellar structures that restrict proton mobility to two-dimensional networks [69–71].

3.10. Antibacterial activity

Different concentrations of cadmium complex $(C_5H_6ClN_2)[CdCl_3H_2O].H_2O$ was applied against two strains, one is Gram-negative (*Klebsiella pneumonia),* and the other is Gram-positive (*Staphylococcus aureus)* using the disc diffusion method, as can be seen in Fig. 11. In the area of inhibition (mm), the compound showed high antibacterial activity against both strains in even small concentrations of 12.5 μg.mL^{-1}. In the case of *Klebsiella pneumonia*, the antibiotics Norfloxacin (NOR-10), Nalidixic acid (NA30) did not inhibit cell viability, but Novobiocin (NV-5) and Erythromycin (E-15) did. In the case of *Staphylococcus aureus*, all four antibiotics used showed a remarkable antibacterial effect. The combination of cadmium complex with the four antibiotics was tested against *K. pneumonia* and *Staphylococcus aureus* using the disc diffusion method. The zone (mm) of inhibition of different antibiotic discs with the $(C_5H_6ClN_2)[CdCl_3H_2O].H_2O$ compound against both strains was measured and showed the highest antimicrobial activity than the free compound or the reference used four antibiotics. Cadmium complex with 50 μg.mL^{-1} produced a maximum fold increase of 60% antibacterial activity against *K. pneumonia* and *S. aureus*. In this study, the antibiotics showed enhanced synergistic activity in the presence of $(C_5H_6N_2Cl)[CdCl_3(H_2O)].H_2O$ against both strains. The increasing antimicrobial activity of the cadmium compound can be explained based on the membrane penetration because there is no charge for the Cd(II) complex and its lipophilicity is greater than that of metal salt. As a result, it can penetrate through the lipid layers of the cell membrane, which causes it to have better antibacterial properties. This can be explained by the fact that there is no charge for the Cd(II) complex [6,72,73].

4. Conclusion

A newly discovered hybrid compound with the formula : $(C_5H_6ClN_2)[CdCl_3H_2O].H_2O$ has been successfully synthesized. In this compound, the organic cations 2-amino-3-chloropyridinium occupy the space contained by the chains of $[CdCl_3(H_2O)]^{n-}_{n}$ and water molecules that make up the framework. Its vibrational properties were investigated through IR spectroscopy, and it was discovered that the compound has semiconducting characteristics and an optical band gap equivalent to 2.8 eV. The low values of the activation energies indicate that protons can assure conduction in this material. Based on the theoretical calculations performed, an attempt was made to provide commentary on the activity of the metal complex. The activity of the metal complex is predicted with the numerical values of the parameters found by both Gaussian calculations and docking calculations. However, ADME analysis of the metal complex predicted its movements in human metabolism. In this investigation, $(C_5H_6ClN_2)[CdCl_3H_2O].H_2O$ increased the antibiotics' synergistic action against both strains, the intense antibacterial activity is consistent with its ability to permeate membranes; since the Cd (II) complex is lipophilic and has no charge, it can pass through cell membrane lipid layers and has greater antibacterial capabilities.

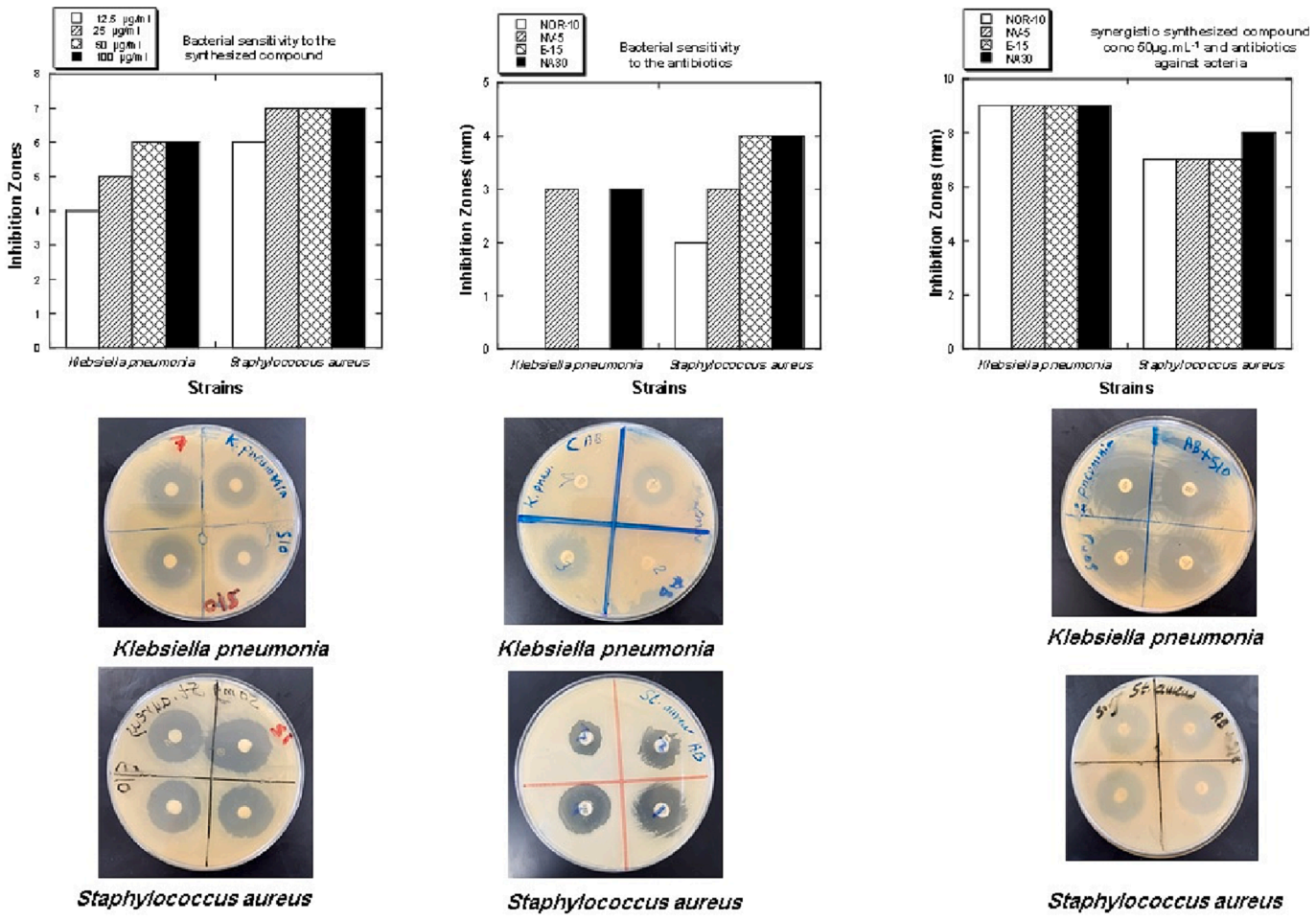

Fig. 11. A) Antimicrobial activity of $(C_5H_6ClN_2)[CdCl_3H_2O].H_2O$ compound (100 µg.mL^{-1}; 50 µg.mL^{-1}; 25 µg.mL^{-1} and 12.5 µg.mL^{-1}) ; b) Antimicrobial activity of the antibiotics Norfloxacin (NOR-10)); Novobiocin (NV-5); Erythromycin (E-15) and Nalidixic acid (NA30) and c) Antimicrobial activity of $(C_5H_6ClN_2)[CdCl_3H_2O].H_2O$ compound combined with the antibiotics.

CRediT authorship contribution statement

Sabrine Hermi: Writing – original draft. **Mohamed Habib Mrad:** Supervision, Visualization. **Abdullah A. Alotaibi:** Methodology, Software. **Burak Tüzün:** Formal analysis. **Uwe Böhme:** Software, Data curation. **Khalid M. Alotaibi:** Resources. **Abdelhak Othmani:** Resources, Investigation. **Hamdy A. Hassan:** Investigation. **Cherif Ben Nasr:** Validation, Investigation.

Declaration of Competing Interest

The authors declare that they have no known competing financial interests or personal relationships that could have appeared to influence the work reported in this paper.

Data availability

No data was used for the research described in the article.

Acknowledgments

- The author would like to thank the Deanship of Scientific Research at Shaqra University for supporting this work.

Appendix A. Supplementary data

Supplementary data to this article can be found online at https://doi.org/10.1016/j.inoche.2023.111122.

References

[1] C. Ayari, A.A. Alotaibi, M.A. Baashen, F. Perveen, A.H. Almarri, K.M. Alotaibi, M. S. Abdelbaky, S. Garcia-Granda, A. Othmani, C.B. Nasr, M.H. Mrad, Materials. (2022), https://doi.org/10.3390/ma15227973.

[2] N. Karâa, B. Hamdi, A.B. Salah, R. Zouari, J. Mol. Struct. (2013), https://doi.org/10.1016/j.molstruc.2013.06.003.

[3] J. Lorenc, I. Bryndal, M. Marchewka, E. Kucharska, T. Lis, and Hanuza, J Raman Spectrosc. (2008), https://doi.org/10.1002/jrs.1925.

[4] Z. Ouerghi, T. Roisnel, R. Fezai, R. Kefi, J. Mol. Struct. (2008), https://doi.org/10.1016/j.molstruc.2018.05.084.

[5] I. Goudiaby, B. Guillot, E. Wenger, S. Soudani, C.B. Nasr, M. Camara, A. Gassama, C. Jelsch, J. Chem. Crystallogr. (2022), https://doi.org/10.1007/s10870-022-00946-0.

[6] M.G. Althobaiti, S. Hermi, A.A. Alotaibi, K.M. Alotaibi, H.A. Hassan, J.X. Mi, C. B. Nasr, M.H. Mrad, Crystals (2022), https://doi.org/10.3390/cryst12020254.

[7] K. Molčanov, B. Kojić-Prodić, IUCrJ. (2019), https://doi.org/10.1107/S2052252519000186.

[8] X. Hu, Z. Li, Y. Ge, S. Liu, C. Shi, Colloids Surf, A Physicochem Eng Asp. (2022), https://doi.org/10.1016/j.colsurfa.2022.128782.

[9] L. Guelmami, M. Hajji, T. Guerfel, Mol. Cryst. (2023), https://doi.org/10.1080/15421406.2023.2194570.

[10] S. Hermi, M.G. Althobaiti, A.A. Alotaibi, A.H. Almarri, W. Fujita, F. Lefebvre, C. Ben Nasr, M.H. Mrad, Crystals (2021), https://doi.org/10.3390/cryst11050553.

[11] W. Cao, Y. Liu, T. Zhang, J. Jia, Polyhedron (2018), https://doi.org/10.1007/s11243-019-00317-3.

[12] C.N. Morrison, K.E. Prosser, R.W. Stokes, A. Cordes, N. Metzler-Nolte, S.M. Cohen, Chem. Sci. (2020), https://doi.org/10.1039/c9sc05586j.

[13] A.H. Rather, T.U. Wani, R.S. Khan, A. Abdal-hay, S.U. Rather, J. Macossay, F. A. Sheikh, Mater. Sci. Eng. B. (2022), https://doi.org/10.3390/ijms232214084.
[14] P.V. Simpson, N.M. Desai, I. Casari, M. Massi, M. Falasca, Future, Med. Chem. (2019), https://doi.org/10.4155/fmc-2018-0248.
[15] G. Gasser, Chimia (2015), https://doi.org/10.2533/chimia.2015.442.
[16] A.D.J. Becke, Chem. phys. (1992), https://doi.org/10.1063/1.462066.
[17] D. Vautherin, D.T. Brink, Spherical nuclei. Phys. Rev C. (1972), https://doi.org/10.1103/PhysRevC.5.626.
[18] E.G. Hohenstein, S.T. Chill, C.D. Sherrill, J. Chem. Theory Comput. (2008), https://doi.org/10.1021/ct800308k.
[19] P. Fuentealba, P. Pérez, R. Contreras, J. Chem. Phys. (2000), https://doi.org/10.1063/1.1305879.
[20] L.H. Lee, Applications of the hard-soft acid-base (HSAB) principle to solid adhesion and surface tribointeractions, in: Surfactants and macromolecules: self-assembly at interfaces and in bulk, Steinkopff, 1990, pp. 337–344.
[21] L.H. Lee, J. Adhes. (1991), https://doi.org/10.1080/00218469108026522.
[22] Y. Li, J.N. Evans, J. Am. Chem. Soc. (1995), https://doi.org/10.1021/ja00134a021.
[23] S. Krishnamurty, R.K. Roy, R. Vetrivel, S. Iwata, S. Pal, J. Phys. Chem. (1997), https://doi.org/10.1021/jp970431c.
[24] R.S. Williams, R. Green, J.N. Glover, Nat. Struct. boil. (2001), https://doi.org/10.1038/nsb1001-838.
[25] Li, H., Fung, K. L., Jin, D. Y., Chung, S. S., Ching, Y. P., Ng, I. O. L., Sun, H., Proteins: Structure, Function, and Bioinformatics. (2007) https://doi.org/10.1002/prot.21361.
[26] K. Okamoto, M. Ikemori-Kawada, A. Jestel, K. von König, Y. Funahashi, T. Matsushima, J. Matsui, ACS Med. Chem. let. (2015), https://doi.org/10.1021/ml500394m.
[27] A.A. Marusiak, N.L. Stephenson, H. Baik, E.W. Trotter, Y. Li, K. Blyth, J. Brognard, Cancer Res. (2016), https://doi.org/10.1158/0008-5472.CAN-15-0701-T.
[28] Stoe& Cie, X-RED and X-AREA. Stoe& Cie, Darmstadt, Germany.
[30] Sheldrick G. M., Acta Cryst., C. (2015) https://doi.org/10.1107/S2053229614024218.
[31] M. Chalkha, A.A. el Hassani, A. Nakkabi, B. Tüzün, M. Bakhouch, A.T. Benjelloun, M. El Yazidi, J. Mol. Struct. (2022), https://doi.org/10.1038/s41598-019-56331-z.
[32] Dennington, R., Keith, T. A., Millam, J. M. (2016). GaussView 6.0. 16. Semichem Inc.: Shawnee Mission, KS, USA.
[33] Frisch M.J., Trucks G.W., Schlegel H.B., Scuseria G.E., Robb M.A., Cheeseman J.R., Scalmani G., Barone V., Mennucci B., Petersson G.A., Nakatsuji H., Caricato M., Li X., Hratchian H.P., Izmaylov A.F., Bloino J., Zheng G., Sonnenberg J.L., Hada M., Ehara M., Toyota K., Fukuda R., Hasegawa J., Ishida M., Nakajima T., Honda Y., Kitao O., Nakai H., Vreven T., Montgomery J.A., Peralta J.E., Ogliaro F., Bearpark M., Heyd J.J., Brothers E., Kudin K.N., Staroverov V.N., Kobayashi R., Normand J., Raghavachari K., Rendell A., Burant J.C., Iyengar S.S., Tomasi J., Cossi M., Rega N., Millam J.M., Klene M., Knox J.E., Cross J.B., Bakken V., Adamo C., Jaramillo J., Gomperts R., Stratmann R.E., Yazyev O., Austin A.J., Cammi R., Pomelli C., Ochterski J.W., Martin R.L., Morokuma K., Zakrzewski V.G., Voth G.A., Salvador P., Dannenberg J.J., Dapprich S., Daniels A.D., Farkas O., Foresman J.B., Ortiz J.V., CioslowskiJ., Fox D.J. (2009). Gaussian 09, revision D.01. Gaussian Inc, Wallingford CT.
[34] A. Tas, B. Tüzün, A.N. Khalilov, P. Taslimi, T. Ağbektas, N.K. Cakmak, J. Mol. Struct. (2022), https://doi.org/10.1016/j.ijbiomac.2018.08.004.
[35] F. Türkan, P. Taslimi, B. Cabir, M.S. Ağırtaş, Y. Erden, H.U. Celebioglu, I. Gulcin, Polycycl. Aromat. Compd. (2022), https://doi.org/10.1080/10406638.2021.1893194.
[36] Ritchie, D., Orpailleur, T. (2013). Hex 8.0. 0 User Manual. Protein Docking Using Spherical Polar Fourier Correlations Copyright c.
[37] S. Salentin, S. Schreiber, V.J. Haupt, M.F. Adasme, M. Schroeder, Nucleic Acids Res. (2015), https://doi.org/10.1093/nar/gkv315.
[38] M.F. Adasme, K.L. Linnemann, S.N. Bolz, F. Kaiser, S. Salentin, V.J. Haupt, M. Schroeder, Nucleic Acids Res. (2021), https://doi.org/10.1093/nar/gkab294.
[39] A. Daina, O. Michielin, V. Zoete, Sci. rep. (2017), https://doi.org/10.1038/srep42717.
[40] A. Daina, V. Zoete, Chem. Med. Chem. (2016), https://doi.org/10.1002/cmdc.201600182.
[41] M. Hajji, T. Guerfel, Chem Res Chin Univ. (2016), https://doi.org/10.1007/s40242-016-5404-3.
[42] M. Hajji, A. Gharbi, T. Guerfel, J. Inorg. Organomet. Polym. (2014), https://doi.org/10.1007/s10904-014-0034-z.
[43] M. HajjIIIi, T. Guerfel, J. Clust. Sci. (2016), https://doi.org/10.1007/s10876-016-1008-9.
[44] W.H. Baur, Acta Cryst. B. (1974), https://doi.org/10.1107/S0567740874004560.
[45] Z.M. Jin, Y.J. Pan, M.L. Hu, S. Liang, J. Chem. Crystallogr. (2001), https://doi.org/10.1023/A:1014391031842.
[46] C.E. Galvez, O.E. Piro, G.A. Echeverría, N.L. Robles, J.O. Lezama, S.V. Sankaran, D. M. Gil, New J. Chem. (2022), https://doi.org/10.1039/D2NJ00428C.
[47] C. Jelsch, K. Ejsmont, L. Huder, IUCrJ (2014), https://doi.org/10.1107/S2052252514003327.
[48] M. Tapera, H. Kekeçmuhammed, B. Tüzün, E. Sarıpınar, Ü.M. Koçyiğit, E. Yıldırım, Y. Zorlu, J. Mol. Struct. (2022), https://doi.org/10.1016/j.molstruc.2022.133816.
[49] M.S. Çelik, Ş.A. Çetinus, A.F. Yenidünya, S. Çetinkaya, B. Tüzün, J. Mol. Struct. (2023), https://doi.org/10.1016/j.molstruc.2022.134158.
[50] A. Günsel, A.T. Bilgiçli, B. Tüzün, H. Pişkin, G.Y. Atmaca, A. Erdoğmuş, M. N. Yarasir, J. Photochem. Photobiol. A. (2019), https://doi.org/10.1016/J.JPHOTOCHEM.2018.12.038.
[52] P.S. Liyanage, R.M. de Silva, K.N. de Silva, J. Mol. Struct. (2003), https://doi.org/10.1016/j.theochem.2005.02.092.
[53] Ü.M. Koçyiğit, M. Doğan, H. Muğlu, P. Taslimi, B. Tüzün, H. Yakan, İ. Gülçin, J. Mol. Struct. (2022), https://doi.org/10.1016/j.molstruc.2022.133249.
[54] B. Bakchi, A.D. Krishna, E. Sreecharan, V.B.J. Ganesh, M. Niharika, S. Maharshi, A. B. Shaik, J. Mol. Struct. (2022), https://doi.org/10.1016/j.bioorg.2019.103522.
[55] O. Alaysuy, H.M. Abumelha, A. Alsoliemy, A. Alharbi, N.M. Alatawi, H.E. Osman, N.M. El-Metwaly, J. Mol. Struct. (2022), https://doi.org/10.1021/ac60203a013.
[56] S. Hermi, A.A. Alotaibi, A.M. Alswieleh, K.M. Alotaibi, M.G. Althobaiti, C. Jelsch, M.H. Mrad, Materials. (2022), https://doi.org/10.3390/ma15051624.
[57] Z. Ouerghi, I. Dridi, T. Roisnel, R. Kefi, J. Mol. Struct. (2021), https://doi.org/10.1016/j.molstruc.2021.130721.
[58] F. Garci, H. Chebbi, A. Klein, M.F. Zid, J. Coord. Chem. (2021), https://doi.org/10.1080/00958972.2021.2024171.
[59] W. Wamani, N. Hannachi, T. Mhiri, M. Belhouchet, Adv. Chem. (2014). https://doi.org/10.24297/jac.v7i2.2364.
[60] C. Ayari, A.A. Alotaibi, M.A. Baashen, K.M. Alotaibi, K.H. Alharbi, A. Othmani, W. Fujita, C.B. Nasr, M.H. Mrad, Crystals (2022), https://doi.org/10.3390/cryst12040486.
[61] Macdonald, J., WB Johnson in: JR Macdonald. Impedance Spectroscopy: Wiley, New York, (1987), 150-170.
[62] W. Wamani, R. Elwej, T. Mhiri, M. Belhouchet, Adv. Chem (2019). https://doi.org/10.24297/jac.v5i3.2663.
[63] K.S. Rao, D.M. Prasad, P.M. Krishna, B. Tilak, K.C. Varadarajulu, Mater Sci Eng B. (2006), https://doi.org/10.1016/j.mseb.2006.06.030.
[64] K.S. Rao, P.M. Krishna, D.M. Prasad, J.H. Lee, J.S. Kim, J. Alloys Compd. (2008), https://doi.org/10.1016/j.jallcom.2007.10.023.
[65] A.M. Sweetman, S.P. Jarvis, H. Sang, I. Lekkas, P. Rahe, Y. Wang, J. Wang, N. R. Champness, L. Kantorovich, P. Moriarty, Nat. Commun. (2014), https://doi.org/10.1038/ncomms4931.
[66] R. Ayouchi, D. Leinen, F. Martın, M. Gabas, E. Dalchiele, J.R. Ramos-Barrado, Thin Solid Films (2003), https://doi.org/10.1016/j.phpro.2014.07.010.
[67] S. Lanfredi, P.S. Saia, R. Lebullenger, A.C. Hernandes, Solid State Ion. (2002), https://doi.org/10.1016/j.nocx.2019.100026.
[68] S. Ghosh, A. Ghosh, Solid State Ion (2002), https://doi.org/10.1016/S0167-2738(02)00170-4.
[69] Alotaibi, A.A., Hermi, S., Perveen, F., Othmani, A., Hassan, H.A., Kaminsky, W., Nasr, C.B. and Mrad, M.H., (2023) https://doi.org/10.1007/s10876-023-02422-x.
[70] M.S. Lee, T. Kim, S.H. Park, C.S. Kim, Y.W. Choi, J Mater Chem. (2012), https://doi.org/10.1039/C2JM32628K.
[71] Z. Mazej, E.A. Goreshnik, Z. Anorg. Allg. Chem. (2015), https://doi.org/10.1002/zaac.201500110.
[72] K.B.A. Ahmed, T. Raman, A. Veerappan, Mater. Sci. Eng. C. (2016), https://doi.org/10.1016/j.msec.2016.06.034.
[73] V. Reddy, N. Patil, T. Reddy, S.D. Angadi, J. Chem. (2008), https://doi.org/10.1155/2008/690535.

Sabrine Hermi, https://orcid.org/0000-0002-4680-3998

Mohamed Habib Mrad, https://orcid.org/0000-0001-5799-7428

Burak Tüzün, https://www.researchgate.net/profile/Burak-Tuezuen

Uwe Böhme, https://www.researchgate.net/profile/Uwe-Boehme

Khalid M. Alotaibi, https://orcid.org/0000-0002-2384-1705

Abdelhak Othmani, https://www.researchgate.net/profile/Abdelhak-Othmani

Abdullah A. Alotaibi, https://www.researchgate.net/profile/Abdullah-Alotaibi-3

Hamdy A. Hassan, https://www.researchgate.net/profile/Hamdy-Hassan-2

Cherif Ben Nasr https://orcid.org/0000-0001-7624-6427